THE JOURNAL OF PHYSICAL CHEMISTRY Letters

pubs.acs.org/JPCL Letter

Quantitative Anisotropic Analysis of Molecular Orientation in Amorphous N_2O at 6 K by Infrared Multiple-Angle Incidence Resolution Spectrometry

Tetsuya Hama,* Atsuki Ishibashi, Akira Kouchi, Naoki Watanabe, Nobutaka Shioya, Takafumi Shimoaka, and Takeshi Hasegawa

Cite This: J. Phys. Chem. Lett. 2020, 11, 7857−7866

Read Online

ACCESS | Metrics & More | Article Recommendations | Supporting Information

ABSTRACT: The existence of molecular orientational order in nanometer-thick films of molecules has long been implied by surface potential measurements. However, direct quantitative determination of the molecular orientation is challenging, especially for metastable amorphous thin films at low temperatures. This study quantifies molecular orientation in amorphous N_2O at 6 K using infrared multiple-angle incidence resolution spectrometry (IR-MAIRS). The intensity ratio of the weak antisymmetric stretching vibration band of the $^{14}N^{15}NO$ isotopomer between the in-plane and out-of-plane IR-MAIRS spectra provides an average molecular orientation angle of 65° from the surface normal. No discernible change is observed in the orientation angle when a different substrate material is used (Si and Ar) at 6 K or the Si substrate temperature is changed in the range of 6−14 K. This suggests that the transient mobility of N_2O during physisorption is key in governing the molecular orientation in amorphous N_2O.

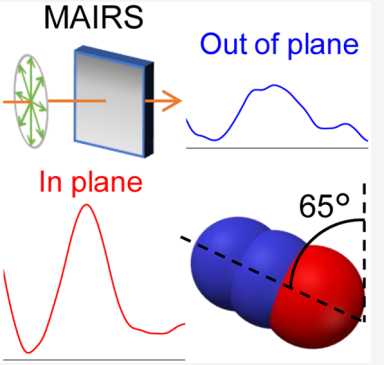

Vapor deposition is used to prepare thin films of metals, semiconductors, and dielectrics in a vacuum, and it has wide-ranging applications across many fields for the development of functional materials.[1−3] Thin-film growth of molecules (e.g., H_2O, CO, CO_2, NH_3, CH_4, and CH_3OH) at low temperatures is also key to understanding the formation in cold interstellar regions at around 10 K of icy dust grains, which are the starting material for the evolution of planetary systems.[4−6] In 1969, Elliott et al. reported the buildup of surface potential during the condensation of water vapor on the surface of a liquid-nitrogen trap.[7] The electrical properties of molecular-solid thin films at low temperatures have been widely investigated for decades, and many polar molecules develop a surface potential during vapor deposition on a cold substrate: for example, H_2O,[8−11] CO,[8,12] NO,[8] N_2O,[8,13,14] SO_2,[8] NH_3,[8] halocarbons ($CHCl_3$,[10] CF_3Cl,[14,15] CF_2Cl_2,[15] $CFCl_3$,[15] $CHCl{=}CCl_2$,[10] and *o*-$C_6H_4Cl_2$ (*ortho*-dichlorobenzene)[10]), and organic compounds (acetone,[8,10] toluene,[10,14] propane,[14] isopentane,[14] isoprene,[14] methyl formate,[16,17] ethyl formate,[18] 2,5-dihydrofuran,[18] and alcohols ($C_nH_{2n+1}OH$, n = 1−5) including isobutanol[10,19−21]); see also review articles.[18,22] N_2O has been extensively studied by Field and co-workers[13,14,18,22−27] because it exhibits a clear change in its surface potential. A positive surface potential of about +11 V was reported for 355 monolayers (MLs) of polycrystalline N_2O at 40 K (+32 mV per ML), which corresponds to an electric field of about 10^8 V m^{-1}.[13,14,18] The authors also reported that the substrate temperature strongly affected the development of the surface potential, with a potential of only about +1 V developing for 355 MLs of polycrystalline N_2O at 65 K.[13,14,18] Because nonpolar molecules such as Ne, Ar, N_2, CO_2, CCl_4, and benzene (C_6H_6) do not induce surface potential evolution,[8,10] the orientational order of polar molecules (dipole alignment) has been proposed as the origin of the electric potential in molecular-solid thin films at low temperatures.

Direct quantitative measurement of molecular orientation in thin solid films is challenging, especially for metastable amorphous molecular solids at low temperatures of around 10 K, despite the relevance of the orientation to the structure of icy dust in cold interstellar regions.[4−6,28] Diffraction techniques using electrons or X-rays provide only limited information about the structure of amorphous materials. Although infrared (IR) spectroscopy is used to study amorphous thin films, conventional measurement techniques, such as normal-incidence transmission (Tr) and reflection−absorption (RA) at grazing incidence using a metallic substrate, observe only the surface-parallel (in-plane; IP) and surface-perpendicular (out-of-plane; OP) components of a transition moment (molecular vibration), respectively, owing

Received: May 22, 2020
Accepted: August 25, 2020

https://dx.doi.org/10.1021/acs.jpclett.0c01585
J. Phys. Chem. Lett. 2020, 11, 7857−7866

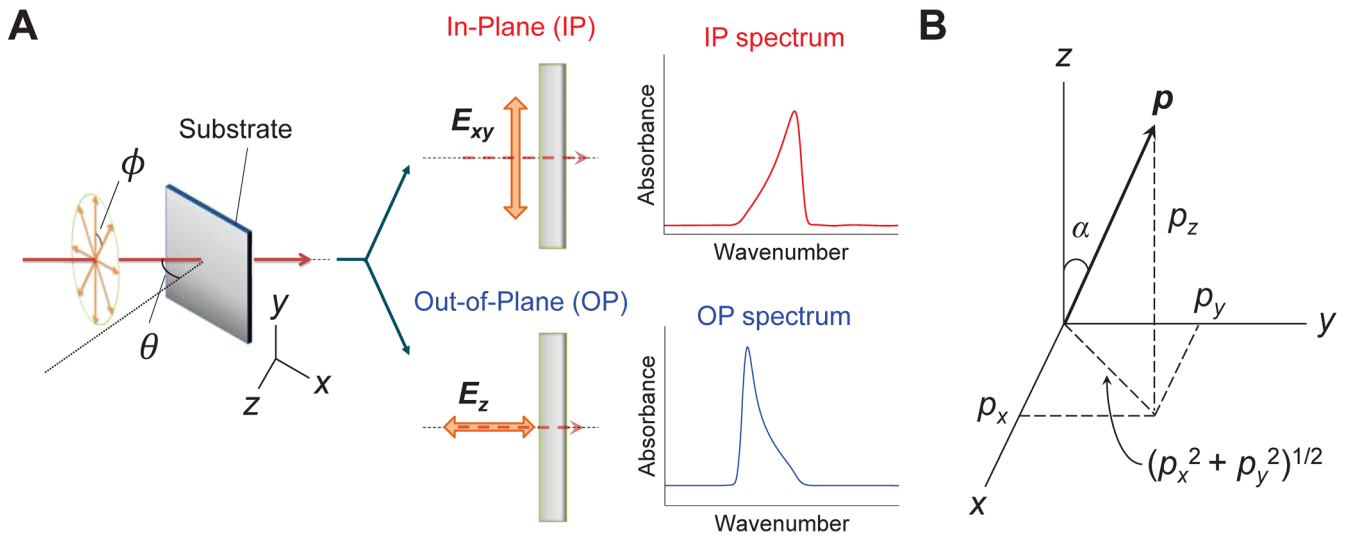

Figure 1. Overview of the IR-MAIRS measurement system. (A) Schematic of the IR-MAIRS measurement. The film is irradiated with linearly polarized IR light at a polarization angle (ϕ) at an angle of incidence of θ. Oblique incidence transmission measurements are performed at $\theta = 45°$ at seven polarization angles from $\phi = 0°$ (s-polarization) to 90° (p-polarization) in 15° steps (see also Figures S1 and S2 in the Supporting Information). The IP and OP components of the single-beam spectra are calculated through the classical least-squares regression equation (see Experimental Methods for details). This system is called MAIRS2 in the original paper.[36] E_{xy} and E_z are the electric fields along the surface-parallel (in-plane) and surface-perpendicular (out-of-plane) direction at the optical interface, respectively. (B) Schematic of a transition moment (***worp***) in Cartesian coordinates. p_i ($i = x$, y, or z) are the x-, y-, and z-direction components for the transition moment. In MAIRS2, a uniaxial system with $p_x = p_y$ is assumed; that is, the orientation angle is determined by an angle about the z axis. α is the uniaxial orientation angle of the transition moment from the surface normal.

to surface selection rules.[29−31] These limitations make an accurate analysis of molecular orientation in amorphous thin films difficult. Consequently, the relationship between the structure and properties of molecular-solid thin films is poorly understood despite the accumulation of surface potential measurements.

IR multiple-angle incidence resolution spectrometry (IR-MAIRS) has recently been developed for the quantitative analysis of the molecular orientation in organic thin films.[30−36] IR-MAIRS is a spectroscopic method coupled with multivariate analysis for retrieving both pure IP and OP vibration spectra from an identical sample simultaneously irrespective of its crystallinity (Figure 1 and Experimental Methods; see also refs 30 and 31 for details). The method has the unique advantage that the average molecular orientation is determined by comparing the IP to OP band intensity ratio spectra on the absorbance scale (A_{IP}/A_{OP}). Despite its potential usefulness, IR-MAIRS has yet to be used for amorphous molecule thin films prepared at low temperatures in a vacuum. In this study, we develop an experimental setup for *in situ* IR-MAIRS in low-temperature, ultrahigh-vacuum conditions (see Experimental Methods). We first validate low-temperature, ultrahigh-vacuum IR-MAIRS using amorphous CH_4 at 6 K, which gives similar IP and OP band intensities in IR-MAIRS because CH_4 is isotropic, and then show the spectroscopic signatures of anisotropic molecular orientation for amorphous N_2O at 6 and 14 K.

Figure 2 shows the IP and OP spectra of amorphous CH_4 obtained in the $\nu 3$ C−H stretching vibration band (A and B) and those of amorphous N_2O in the $\nu 3$ antisymmetric stretching vibration band (C and D) on a Si substrate at 6 K as a function of gas exposure time. We used a recently developed technique, MAIRS2,[36] to obtain the IP and OP spectra with better signal-to-noise ratios than conventional MAIRS techniques (Figure 1 and Experimental Methods). Hereafter, MAIRS2 is simply referred to as MAIRS. Similar band intensities between the IP and OP spectra at each exposure time for 1−128 min indicate the isotropic nature of CH_4 (Figure 2A,B). IR-MAIRS yields the intensity ratio of the surface-parallel (x- and y-directions) and surface-perpendicular (z-direction) components of a transition moment via the IP and OP spectra, and the orientation angle, α, is defined as the uniaxial orientation angle of the transition moment, $\boldsymbol{p}$, from the surface normal (Figure 1B). Assuming a uniaxial distribution, where the distribution of the transition moments in the x−y plane, p_x and p_y, is averaged so that $p_x = p_y$ (Figure 1), the orientation angle α can be obtained by eq 1 because absorbance is proportional to the square of the transition moment (Fermi's golden rule) (see refs 30 and 31 for details).

$$\tan\alpha = \frac{\sqrt{p_x^{\,2} + p_y^{\,2}}}{p_z} = \frac{\sqrt{2}\,p_x}{p_z} = \sqrt{\frac{2A_{IP}}{A_{OP}}} \qquad (1)$$

Unlike conventional measurement techniques, IR-MAIRS enables us to perform molecular orientation analysis without the need for optical parameters of thin sample films, because it retrieves the pure IP and OP components from the experimentally measured single-beam spectra as the least-squares solution of the classical least-squares regression equation (see Experimental Methods and refs 30−36 for details). The accuracy of IR-MAIRS can be further improved by considering the effect of the refractive index (n) of the thin film on the intensities of the electric fields at the optical interface along the surface-parallel (E_{xy}) and surface-perpendicular (E_z) directions (Figure 1A).[30,35] Shioya et al.[36] theoretically deduced the correction factor to account for the intensity ratio of the electric fields at the optical interface (E_{xy}/E_z) to improve the molecular orientation analysis and modified eq 1 to correct the band intensity of the OP spectrum as

https://dx.doi.org/10.1021/acs.jpclett.0c01585
J. Phys. Chem. Lett. 2020, 11, 7857−7866

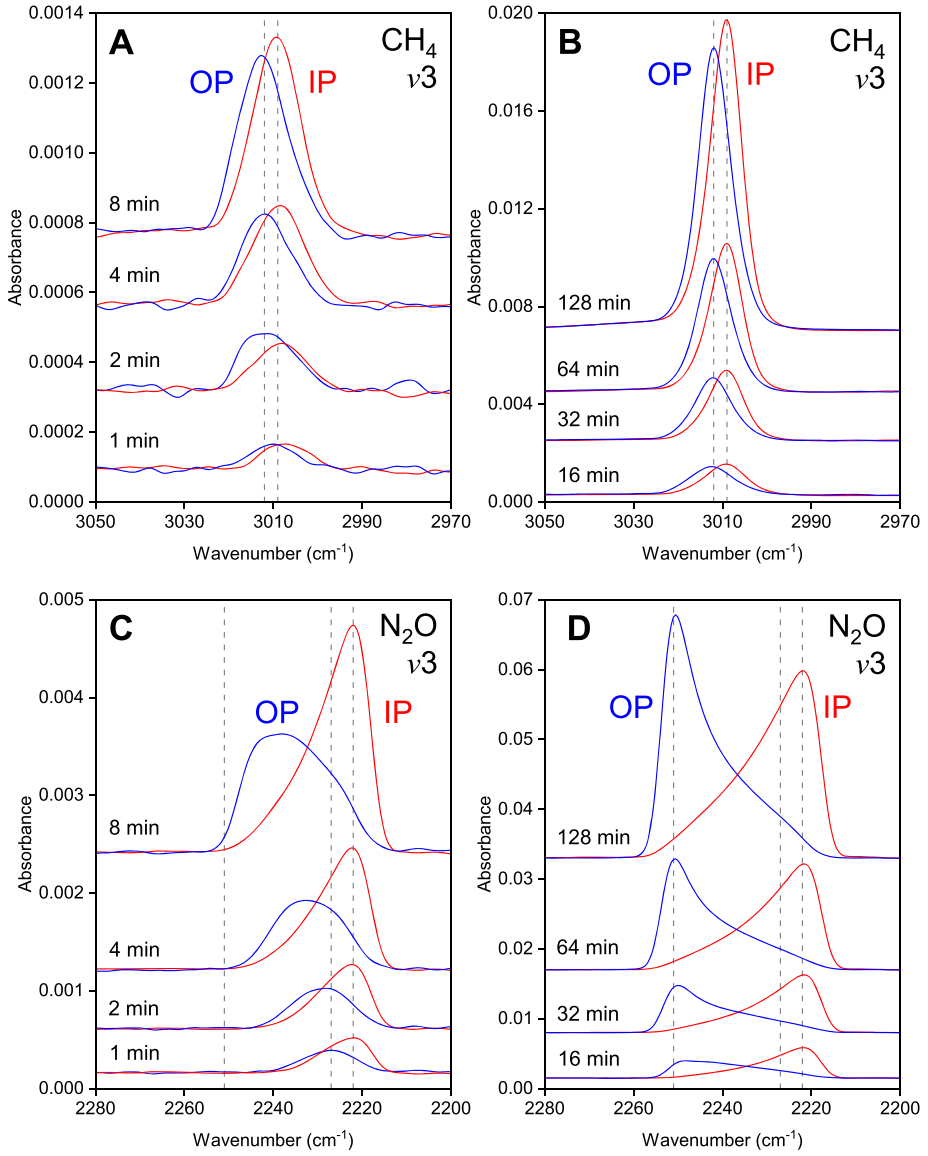

Figure 2. IP and OP spectra obtained by IR-MAIRS as a function of gas exposure time. (A and B) $\nu 3$ C−H stretching vibration band of amorphous CH_4 at 6 K. The dashed gray guidelines are at 3012 and 3009 cm^{-1}. (C and D) $\nu 3$ antisymmetric stretching vibration band of amorphous N_2O at 6 K. The dashed gray guidelines are at 2251, 2227, and 2222 cm^{-1}. The pressure in the chamber is 6.7×10^{-6} and 6.0×10^{-6} Pa during CH_4 and N_2O exposure, respectively.

$$\tan \alpha = \sqrt{\frac{2A_{IP}}{n^4 H A_{OP}}} \quad (2)$$

where H is the substrate-specific parameter (0.33 for Si).[36] In this study, typical refractive indices of 1.30 (n^4H = 0.943) and 1.32 (n^4H = 1.002) are used for the OP spectra of amorphous CH_4 and N_2O, respectively, unless otherwise stated.[37−39] The figures in this Letter show the corrected band intensities for the OP spectra by multiplying n^4H.

Figure 3 shows the orientation angles from the surface normal obtained from the $\nu 3$ band of amorphous CH_4 at 6 K in Figure 2A,B. The calculated orientation angles are around α = 56° after 8−128 min of exposure (see also Table S1 in the Supporting Information). This angle is close to the angle of 54.7°, which indicates a perfectly random orientation angle. We also tested the dependence of the n value in solid CH_4 on the orientation angle, using reported values of 1.28,[38] 1.33,[40] and 1.36.[41,42] Figure 3 shows that the orientation angles are calculated as α = 56.4° and 53.1° for n = 1.28 and 1.36 ($0.886 \le n^4H \le 1.129$) after 128 min of exposure, respectively (see also Table S2 in the Supporting Information). IP and OP spectra exhibit almost identical band intensity when n = 1.33, which gives α = 54.3° (see also Figure S3 in the Supporting Information). These results verify that the MAIRS system provides average orientation angle α with an accuracy of ±2°, when the refractive index (n) is available.

The IP and OP spectra obtained by IR-MAIRS correspond to the Tr and RA spectra, respectively, in terms of shape and band positions because they are expressed as transverse (TO) energy-loss functions (=$2nk$) and longitudinal (LO) optic energy-loss functions $\left(= \frac{2nk}{(n^2 + k^2)^2} \right)$, respectively,[29−31,36,43] where n and k are the real and imaginary parts of the complex refractive index ($n + ik$) of the thin film in IR regions, respectively. The band shape and peak position of the $\nu 3$ band (3009 cm^{-1}) in the IP spectra agree well with that in the Tr

https://dx.doi.org/10.1021/acs.jpclett.0c01585
J. Phys. Chem. Lett. 2020, 11, 7857−7866

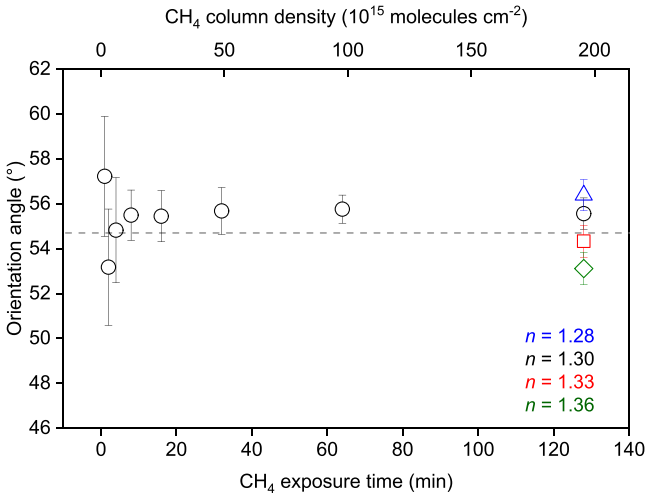

Figure 3. Calculated average orientation angle of the transition moment from the surface normal. (A) ν3 C−H stretching vibration band of amorphous CH_4 on a Si substrate at 6 K assuming n = 1.28 (open triangle), 1.30 (open circles), 1.33 (open square), and 1.36 (open diamond). The dashed gray guidelines are at the angle of 54.7° indicating random orientation.

spectra for amorphous CH_4 at 8 K (3010 cm^{-1}).[38] In contrast, the OP spectra exhibit different peak positions at 3012 cm^{-1} after 128 min of exposure (Figure 2A, B). This IP−OP peak shift originates from the TO−LO splitting, which is induced by the dispersion of n induced by the large k values, namely, the strong absorption.[31,43] According to Gerakines and Hudson,[38] the ν3 band of amorphous CH_4 has a large k value (0.63) at 3010 cm^{-1} compared with a typical k value (0.3) for organic compounds (e.g., $CH_3(CH_2)_{17}SH$) in the $\nu_{as}(CH_2)$ antisymmetric stretching vibration band at 2918 cm^{-1}.[29,44] This is consistent with the larger IP−OP peak shift in the ν3 band ($\Delta\tilde{\nu}$ = 3 cm^{-1}) of amorphous CH_4 than that in the $\nu_{as}(CH_2)$ band of cadmium stearate ($\Delta\tilde{\nu} \leq 1$ cm^{-1}) in IR-MAIRS.[33,45]

In contrast to the MAIRS results in amorphous CH_4, the IP and OP spectra of amorphous N_2O show substantially different band shapes and intensities (Figure 2C,D). The ν3 peak positions of the IP spectra stay at 2222 cm^{-1} throughout the N_2O exposure for 128 min, which agrees well with the reported peak wavenumber for the Tr spectrum of amorphous N_2O at 10 K (2222 cm^{-1}).[39] Because the Tr spectrum of crystalline N_2O has a different ν3 peak position at 2237 cm^{-1},[39] the present solid N_2O samples at 6 K are amorphous throughout the 128 min gas exposure. Nevertheless, the peak positions of the OP spectra change from 2227 cm^{-1} ($\Delta\tilde{\nu}$ = 5 cm^{-1}) to 2251 cm^{-1} ($\Delta\tilde{\nu}$ = 29 cm^{-1}) during 1−128 min of exposure. The band intensity ratio of IP to OP spectra also changes as a function of the N_2O exposure time (see Table S3 in the Supporting Information). The IP spectra have stronger band intensities than the OP spectra (Figure 2C) during 1−32 min of exposure (8.3×10^{14}−2.7×10^{16} molecules cm^{-2}), whereas the A_{IP}/A_{OP} ratio decreases as the exposure time increases. The band intensity of the OP spectra eventually becomes stronger than that of the IP spectra at 128 min (1.1×10^{17} molecules cm^{-2}) (Figure 2D).

In strongly absorbing bands having a k value greater than typically 1, an oscillating local electric field created by the vibrational motion of an N_2O molecule in the solid phase affects the transition dipoles in the surrounding N_2O molecules. An example of such a band is the ν3 band of N_2O, whose k value is as large as 1.85 at $\tilde{\nu}$ = 2222 cm^{-1} based on the reported absorption coefficient ($4\pi k\tilde{\nu}$ = 51 580 cm^{-1}).[39] Ovchinnikov and Wight reported that the N_2O molecular vibrations in the ν3 band are delocalized throughout amorphous N_2O by dipole−dipole interactions between the vibrations of the molecules.[46] We therefore conclude that the molecular orientation analysis based on the strong ν3 band is

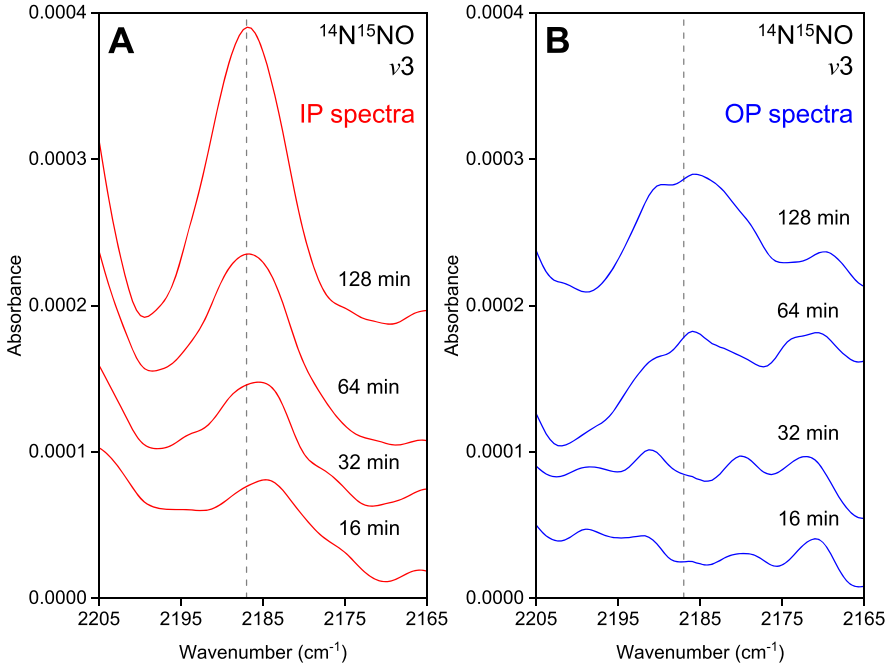

Figure 4. IR-MAIRS for solid N_2O at 6 K in the region of the ν3 ($^{14}N^{15}NO$) isotope band as a function of exposure time at 6.0×10^{-6} Pa. (A) IP spectra and (B) OP spectra. The dashed gray guidelines are at 2187 cm^{-1}.

https://dx.doi.org/10.1021/acs.jpclett.0c01585
J. Phys. Chem. Lett. 2020, 11, 7857−7866

Table 1. Summary of A_{IP}, n^4HA_{OP}, $\sqrt{\frac{2A_{IP}}{n^4HA_{OP}}}$, and Orientation Angle α for the $^{14}N^{15}NO$ ν3 Band of Amorphous N_2O[a]

experiment	A_{IP}	error bar	n^4HA_{OP}	error bar	$\sqrt{\frac{2A_{IP}}{n^4HA_{OP}}}$	error bar	orientation angle α (deg)	error bar (deg)
Si at 6 K[b]	2.15×10^{-3}	0.07×10^{-3}	0.93×10^{-3}	0.13×10^{-3}	2.16	0.15	65.1	1.5
Si at 6 K[b] $n = 1.42$ $n^4H = 1.342$	2.15×10^{-3}	0.07×10^{-3}	1.25×10^{-3}	0.17×10^{-3}	1.87	0.13	61.7	1.7
Ar at 6 K[c]	2.03×10^{-3}	0.07×10^{-3}	0.97×10^{-3}	0.18×10^{-3}	2.07	0.19	64.1	2.0
Si at 14 K[d]	2.16×10^{-3}	0.013×10^{-3}	0.84×10^{-3}	0.11×10^{-3}	2.27	0.18	66.2	1.7

[a]The band intensities of the IP and OP spectra (A_{IP} and A_{OP}, respectively) are calculated using the peak area of the $^{14}N^{15}NO$ ν3 band of amorphous N_2O. A typical refractive index of $n = 1.32$ is used for the calculation of n^4HA_{OP} unless otherwise stated, where H is the substrate-specific parameter ($H = 0.33$ for Si, and thus, $n^4H = 1.002$). [b]Amorphous N_2O on a Si substrate at 6 K formed by 128 min of exposure at 6.0×10^{-6} Pa, which corresponds to an exposure of 1.1×10^{17} molecules cm^{-2}. [c]Ar film was prepared on a Si substrate at 6 K by gas exposure at 7.3×10^{-6} Pa for 2 min (2.1×10^{15} molecules cm^{-2}), and amorphous N_2O was subsequently formed by 128 min of exposure at 6.0×10^{-6} Pa. [d]Amorphous N_2O on a Si substrate at 14 K formed by 128 min of exposure at 6.0×10^{-6} Pa.

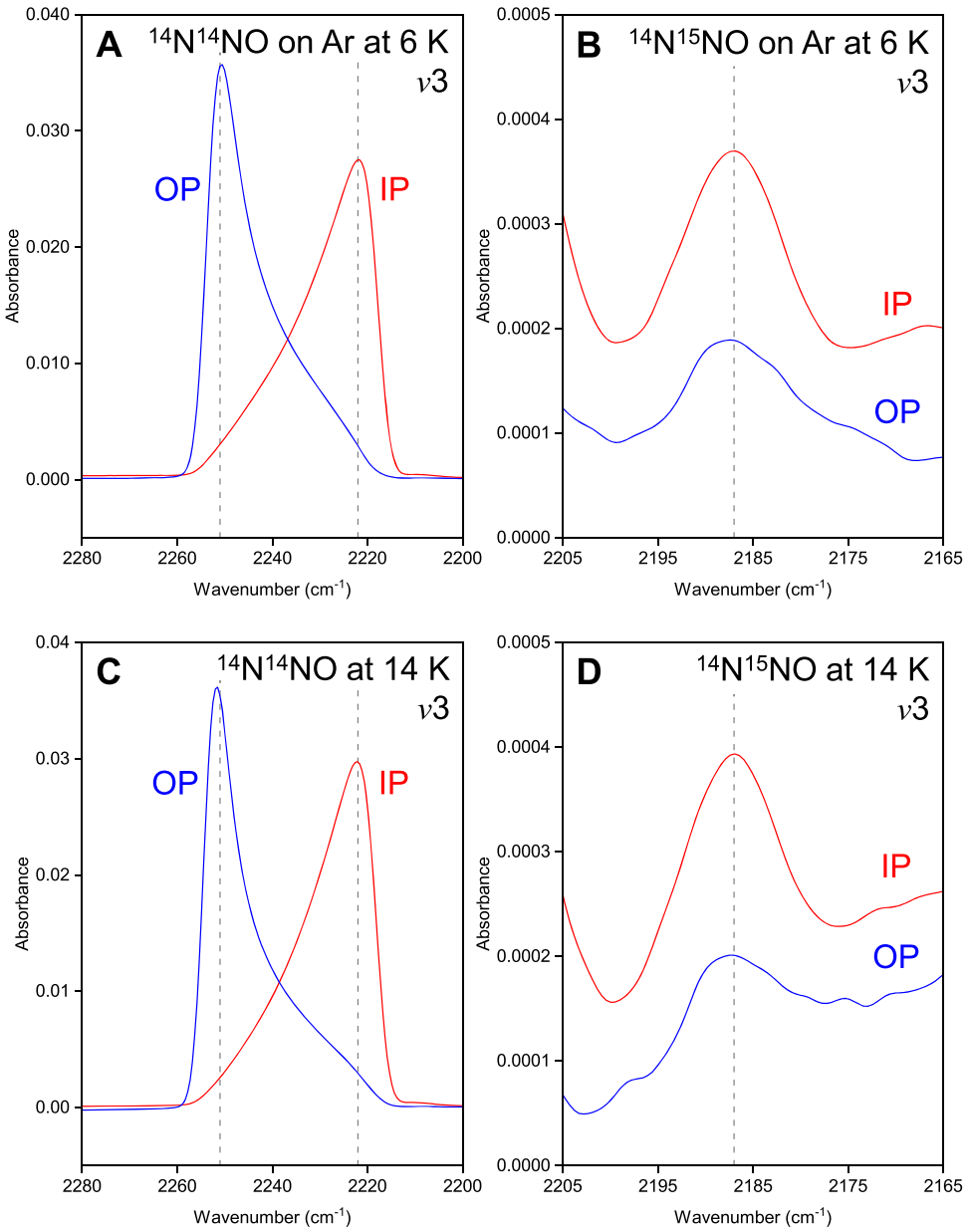

Figure 5. IP and OP spectra of the ν3 band of amorphous N_2O. (A and B) Amorphous N_2O on an Ar thin film at 6 K. The Ar film was prepared on a Si substrate at 6 K by gas exposure at 7.3×10^{-6} Pa for 2 min, and amorphous N_2O was formed by 128 min of exposure at 6.0×10^{-6} Pa. (A) $^{14}N^{14}NO$ and (B) $^{14}N^{15}NO$. (C and D) Amorphous N_2O on a Si substrate at 14 K formed by 128 min of exposure at 6.0×10^{-6} Pa. (C) $^{14}N^{14}NO$ and (D) $^{14}N^{15}NO$. The dashed gray guidelines are at 2251 and 2222 cm^{-1} (A and C) and 2187 cm^{-1} (B and D), for reference.

https://dx.doi.org/10.1021/acs.jpclett.0c01585
J. Phys. Chem. Lett. 2020, 11, 7857−7866

inappropriate. Ovchinnikov and Wight also suggested that the line shape of the $\nu 3$ band depends on the macroscopic shape and orientation of the sample owing to the long-range nature of the dipole−dipole interactions. This implies that both the band shape and intensity can differ between the OP and IP spectra in IR-MAIRS, irrespective of molecular orientation.[43,47] We therefore speculate that some morphological changes occur in amorphous N_2O as the film thickness increases during gas deposition over 1−128 min, leading to the change of the band shape and intensity of the OP spectra (Figure 2C,D).[29,48]

In addition, the vibrational Stark effect can induce a frequency shift in the $\nu 3$ band of N_2O, because an electric field can be applied across amorphous N_2O film owing to anisotropic molecular orientation (dipole alignment).[22,25] The vibrational Stark effect on molecular-solid thin films at low temperatures has been studied for polycrystalline N_2O.[22,25] Lasne et al. reported that the vibrational Stark effect can enlarge the TO−LO splitting ($\Delta\tilde{\nu}_{TL}$) in polycrystalline N_2O, which can account for about 30% (5.2 cm^{-1}) and 10% (1.4 cm^{-1}) of the total TO−LO splitting at 48 K ($\Delta\tilde{\nu}_{TL}$ = 17.2 cm^{-1}) and 66 K ($\Delta\tilde{\nu}_{TL}$ = 13.4 cm^{-1}), respectively.[25] The vibrational Stark effect is yet to be studied for amorphous N_2O because of strong inhomogeneous spectral broadening by the long-range dipole−dipole interactions,[25,46] which makes a reliable analysis of small shifts of the TO and LO peak positions difficult as a function of deposition temperature (typically 1−2 cm^{-1} at 48−66 K for polycrystalline N_2O).[25] IR-MAIRS is potentially useful to study the TO-LO splitting, because it can obtain TO and LO energy-loss functions as IP and OP spectra, respectively, from an identical sample irrespective of its crystallinity. However, a comprehensive understanding of the shape and intensity in the $\nu 3$ band of the IP and OP spectra for amorphous N_2O requires a more detailed future investigation. Both surface potential measurements and microscopic observations of nano- or micrometer scale structures of amorphous N_2O are highly desirable to elucidate the influences of the vibrational Stark effect and long-range dipole−dipole interactions on the IP and OP spectra, which are beyond the scope of this Letter.

To obtain information about molecular orientation, we thus focused on the weak $\nu 3$ band of the $^{14}N^{15}NO$ isotopomer at 2187 cm^{-1}.[46] The $^{14}N^{15}NO$ $\nu 3$ band is spectrally isolated and off-resonance with the major $^{14}N^{14}NO$ $\nu 3$ band, and its concentration (0.37%)[49] is sufficiently low for intermolecular vibrational coupling to be ignored (Figure 4). Therefore, the $\nu 3$ band of the $^{14}N^{15}NO$ isotopomer can be regarded as an uncoupled localized vibration, and its transition moment direction reflects the molecular orientation of $^{14}N^{15}NO$ molecules in amorphous N_2O. The $\nu 3$ band of the $^{14}N^{15}NO$ isotopomer was detected in the IP spectrum after N_2O exposure for 16−32 min (Figure 4A), although the corresponding OP spectrum does not show a peak (Figure 4B). The $^{14}N^{15}NO$ $\nu 3$ band appeared in the OP spectra after 64−128 min of exposure of N_2O; however, their band intensities are weaker than those in the IP spectra. These results show that the IP component of the transition moment of the $^{14}N^{15}NO$ $\nu 3$ band is stronger than the OP component in amorphous N_2O at 6 K throughout the 16−128 min of exposure. The peak positions in the $^{14}N^{15}NO$ $\nu 3$ band are similar between the IP and OP spectra at 2187 cm^{-1} (Figure 4),[39,46] indicating a negligible contribution of intermolecular vibrational coupling. Hence, the intensity ratio of the $^{14}N^{15}NO$ $\nu 3$ band between the IP and OP spectra provides the molecular orientation angle. The orientation angle, α, was calculated as 65.1° ± 1.5° from the surface normal using eq 2 (Table 1). The present MAIRS results thus quantitatively show that there is an anisotropic molecular orientation even in an amorphous material at 6 K. The obtained orientation angle α in amorphous N_2O is an average over the area irradiated by polarized IR light (about 20 mm diameter). For reference, we tested the dependence of the n value in amorphous N_2O on the orientation angle, using a reported value of 1.42 for polycrystalline N_2O (Table 1).[39] The orientation angle is calculated as α = 61.7° ± 1.7°, which is still greater than 54.7° indicating random orientation. Note that the refractive index of the amorphous N_2O in this study should be close to the reported value in Hudson et al. (n = 1.32),[39] because the pressures for N_2O exposure are similar to each other at 10^{-6}−10^{-5} Pa.

To investigate the effect of the substrate on the molecular orientation in amorphous N_2O, we prepared thin films of Ar on the Si substrate at 6 K by gas deposition at 7.3 × 10^{-6} Pa for 2 min (2.1 × 10^{15} molecules cm^{-2}) before the formation of amorphous N_2O. For reference, there are about 1.4 × 10^{15} molecules cm^{-2} on the surface of crystalline Ar, considering that there are four molecules in a unit cell with lattice parameters of a = 5.30 Å.[50] Hence, 2.1 × 10^{15} molecules cm^{-2} correspond to about 1 ML, which is suitable for investigating the influence of the substrate−adsorbate interaction without changing the surface morphology significantly. Figure 5 shows the IP and OP spectra in the $\nu 3$ band region of (A) $^{14}N^{14}NO$ and (B) $^{14}N^{15}NO$ in amorphous N_2O on the Ar thin film at 6 K. Because the thickness of the Ar film (about 1 ML) is much smaller than that of the amorphous N_2O (about 100 ML), the refractive index of amorphous N_2O (n = 1.32) was used for the OP spectra as a good approximation (Table 1). The IP and OP spectra of $^{14}N^{14}NO$ and $^{14}N^{15}NO$ isotopomers have band shapes and intensities almost identical to the corresponding spectra on the bare Si substrate (Figures 2D and 4), and the $^{14}N^{15}NO$ $\nu 3$ band exhibits a similar orientation angle (α = 64.1° ± 2.0°) (Table 1). These results suggest that the molecular orientation is determined by physisorption of N_2O molecules on the surface through van der Waals forces in this study. The independence of the electrical properties in molecular solids from the substrate is also reported in previous studies.[8,18,24]

Because N_2O is a triatomic linear molecule, an orientation parallel to the surface is thermodynamically preferred for physisorbed N_2O because of the large contact area with the surface. The physical vapor deposition of linear-chain molecules (e.g., paraffin and stearic acid) on a cold substrate generally results in a parallel molecular orientation to achieve a large surface contact area.[1,51,52] Compared with linear-chain molecules, the energy difference for physisorbed N_2O between parallel and perpendicular orientations to the surface is much smaller. Nevertheless, the small anisotropic difference in the physisorption energy of N_2O is attributed to the slightly parallel molecular orientation (65°) in amorphous N_2O, especially at a low temperature of 6 K.

From the kinetic point of view, the formation of metastable amorphous N_2O at 6 K shows that the incoming N_2O molecules cannot diffuse and settle on the most energetically favorable crystalline sites until new monomers are adsorbed and molecular motion ceases.[53] Considering the random orientation of N_2O molecules in the gas phase, the transient diffusion of adsorbed N_2O before it is fully thermalized on the

https://dx.doi.org/10.1021/acs.jpclett.0c01585
J. Phys. Chem. Lett. 2020, 11, 7857−7866

surface leads to the parallel molecular orientation ($\alpha = 65°$) in amorphous N_2O at 6 K. When the N_2O deposition experiment is performed on the Si substrate at 14 K, a similar orientation angle ($\alpha = 66.2° \pm 1.7°$) is obtained for the $^{14}N^{15}NO$ $\nu 3$ band of amorphous N_2O (Figure 5D; see also Table S4 in the Supporting Information). Hence, at substrate temperatures of 6−14 K, the transient mobility of the adsorbed N_2O molecules is driven by the incident kinetic temperature (295 K) and the physisorption energy on the surface, rather than the substrate temperature. Thus, molecular dynamics during physisorption is a key factor in the molecular orientation of amorphous N_2O. The physisorption energy of N_2O should lie in the range of 1000−3500 K, considering the physisorption energy of the N_2O−N_2O dimer (903−929 K),[54] the desorption energy of polycrystalline CO_2 (2300−3500 K),[55,56] and similar desorption temperatures between polycrystalline CO_2 and N_2O at substrate temperatures of 70−95 K.[13,18,55,56] Further evaluation of the role of the physisorption process in the observed parallel molecular orientation requires molecular dynamics simulations. Above 22 K, N_2O starts to crystallize, which makes the IR spectra of the solid N_2O sample unstable because the N_2O crystallization is not completed during MAIRS measurements for 2611 s (see Experimental Methods for details).

Finally, we discuss the present results by comparing them with previous studies of surface potential measurements. In 1972, Kutzner reported that the positive surface potential of solid N_2O has a maximum at around 40 K between 3 and 100 K.[8] Plekan et al. quantified the ratio of the average surface-normal component of the dipole moment to the total dipole moment of N_2O in the solid state ($\frac{\langle\mu\rangle_z}{\mu}$) between 38 and 65 K.[14] They showed that $\frac{\langle\mu\rangle_z}{\mu} = 0.152$ at 38 K, which corresponds to an electric field of about 1.189×10^8 V m^{-1}, and $\frac{\langle\mu\rangle_z}{\mu}$ decreases monotonically with increasing surface temperature; $\frac{\langle\mu\rangle_z}{\mu} = 0.0204$ at 65 K (1.598×10^7 V m^{-1}).[14] The $\frac{\langle\mu\rangle_z}{\mu}$ value of N_2O at 6 K is estimated as 0.02−0.03 (1.6−2.4×10^7 V m^{-1}) using Kutzner's experimental curve at 3−100 K, with a $\frac{\langle\mu\rangle_z}{\mu}$ value of 0.152 at 38 K reported by Plekan et al.[14] The $\frac{\langle\mu\rangle_z}{\mu}$ values at 6, 38, and 65 K correspond to the average dipole orientation angles of $\alpha = 88°$−$89°$, 81°, 89° from the surface normal, respectively, calculated from $\cos^{-1}\left(\frac{\langle\mu\rangle_z}{\mu}\right)$ neglecting the cancellation of the dipole moments in N_2O solids.[22] These orientation angles indicate much stronger parallel orientations of solid N_2O molecules to the surface than the orientation angle obtained in this study ($\alpha = 65.1° \pm 1.5°$). In addition, the orientation angle of $\alpha = 65° \pm 2°$ gives a $\frac{\langle\mu\rangle_z}{\mu}$ value of 0.42 ± 0.03 that is too large when dipole-moment cancellation is neglected. Because the contribution of dipole-moment cancellation cannot be discussed based only on the surface potential measurements, it is difficult to consider molecular orientation quantitatively. The present IR-MAIRS results suggest that the cancellation of the N_2O dipole moments should occur on a macroscopic scale in amorphous N_2O, leading to a small degree of net polarization and a positive surface potential at 6 K.[8]

IR-MAIRS allows this approach to be extended to combination studies that include surface potential measurements, and the approach is applicable to all polar molecules studied previously,[8−22] as well as nonpolar molecules, including those with anisotropic molecular shapes (e.g., linear alkanes).[3,33,36,43] Further combination studies using these molecules will provide insights into the origins of the anisotropic molecular orientation and partial dipole alignment during vapor deposition of molecules on cold substrates. IR-MAIRS measurements should also help to reveal the fine structures of solid molecules (e.g., H_2O) that are important to astrophysics at low temperatures because many of these molecules form amorphous solids in cold interstellar regions.

EXPERIMENTAL METHODS

MAIRS Measurements. For low-temperature, ultrahigh-vacuum IR-MAIRS, we built an experimental apparatus comprising a vacuum sample chamber and a Fourier transform infrared (FTIR) spectrometer. The vacuum sample chamber was evacuated to ultrahigh-vacuum conditions (base pressure 10^{-7} Pa) using a turbo molecular pump (STP-451, 480 L s^{-1} for N_2, Edwards). A Si(111) substrate (40 × 40 × 1 mm, Pier Optics Co., Ltd.) was mounted on a copper sample holder without removing the native oxide on the Si surface. The Si substrate and copper sample holder were connected with indium solder by ultrasonic soldering under a nitrogen atmosphere to ensure good thermal contact for cooling the Si substrate to 6 K (Figure S4).[57] The copper sample holder was connected to the cold head of a closed-cycle He refrigerator (RDK-101D, Sumitomo Heavy Industries) and installed in the vacuum sample chamber using a bore-through rotary feedthrough (KRP-152, Kitano Seiki Co., Ltd.).

The Si substrate in the chamber was installed in the sample compartment of the FTIR spectrometer (Nicolet iS50, Thermo Fisher Scientific) in transmission geometry across two ZnSe windows (t = 3 mm) in the chamber. Because the He refrigerator was freely rotatable by the bore-through rotary feedthrough, the angle of incidence of the IR beam (θ) was varied by rotating the Si substrate. The temperature of the Si substrate was measured using a Si diode sensor (DT-670, Lakeshore) placed in the copper sample holder and controlled with an accuracy of ±0.2 K using a temperature controller (Model 325, Lakeshore) and a ceramic heater (40 W).

CH_4 (>99.95%, Nihonsanso Co., Ltd.), N_2O (99.9%, Koike medical Co., Ltd.), and Ar (>99.9995%, Air Water Inc.) were introduced onto the Si substrate at 6 K by background deposition at 1.0×10^{-5} Pa, measured using a crystal ion gauge (M-336MX, Canon Anelva). Molecular-solid thin films are formed on both sides of the Si substrate. The actual pressures for CH_4, N_2O, and Ar were calculated as 6.7×10^{-6}, 6.0×10^{-6}, and 7.3×10^{-6} Pa, respectively, using the gas correction factors for CH_4 (1.49), N_2O (1.66), and Ar (1.37).[58] The fluxes of CH_4, N_2O, and Ar were estimated as 2.6×10^{13}, 1.4×10^{13}, and 1.8×10^{13} molecules cm^{-2} s^{-1}, respectively, based on the actual pressure. For reference, there are about 1.2×10^{15}, 1.2×10^{15}, and 1.4×10^{15} molecules cm^{-2} on the surface of crystalline N_2O, CH_4, and Ar, respectively, considering that there are four molecules in a unit cell with lattice parameters of a = 5.67, 5.85, and 5.30 Å, respectively.[50,59,60] Typical time to achieve the base pressure after deposition is about 5 min.

For IR-MAIRS measurements, the MAIRS2 technique, which was recently developed as the second generation of MAIRS by Shioya et al.,[36] was used. In MAIRS2, the IR spectra

https://dx.doi.org/10.1021/acs.jpclett.0c01585
J. Phys. Chem. Lett. 2020, 11, 7857−7866

of a sample film are collected at a fixed incident angle of θ = 45° with seven polarization angles (ϕ) from s-polarization (ϕ = 0°) to p-polarization (ϕ = 90°) in 15° steps (Figures 1, S1, and S2), and the IP and OP spectra are calculated through the classical least-squares regression equation (see MAIRS Analysis below for details). For reference, the present apparatus can also perform other MAIRS techniques, such as pMAIRS, in which the IR spectra of a sample film on the Si substrate are collected with different incident angles, θ, of 9−44° in 5° steps using p-polarized IR light (see refs 35, 43, and 61 for details). Compared with pMAIRS, MAIRS2 has the advantage that optical interference fringes from multiple reflections in the substrate do not appear in the absorption spectrum because of the oblique incident angle fixed at θ = 45°, which leads to a better signal-to-noise ratio than pMAIRS.[36] The modulated IR light was passed through an angle-controllable wire-grid linear ZnSe polarizer incorporated in the spectrometer before entering the vacuum sample chamber. A mercury cadmium telluride detector was used to detect the IR light. The accumulation number of the single-beam measurements was 500 (373 s) for each polarization angle with a resolution of 4 cm^{-1}. The total measurement time was 2611 s for one IR-MAIRS measurement.

MAIRS Analysis. The basic concept of MAIRS is described by Hasegawa[32] and elsewhere.[30,31] The details of the analytical procedure in MAIRS2 used in this study are described by Shioya et al.[36] The analytical expressions for MAIRS deduced from Maxwell's equations are presented by Itoh et al.,[34] although it requires heavy mathematical calculations. Hence, only a brief outline is given here. The intensity of linearly polarized IR light with polarization angle ϕ and incident angle θ (fixed at 45° in this study) are expressed as a linear combination of the IP and OP polarization components (Figure 1A).[32,36] Thus, the experimentally measured single-beam spectra can be decomposed into the pure IP and OP components as the least-squares solution of the classical least-squares regression equation as

$$\mathbf{S}_{obs} = \begin{pmatrix} \mathbf{s}_{obs,1} \\ \mathbf{s}_{obs,2} \\ \vdots \end{pmatrix} = \begin{pmatrix} r_{IP,1} & r_{OP,1} \\ r_{IP,2} & r_{OP,2} \\ \vdots & \vdots \end{pmatrix} \begin{pmatrix} \mathbf{S}_{IP} \\ \mathbf{S}_{OP} \end{pmatrix} + \mathbf{U} \equiv \mathbf{R} \begin{pmatrix} \mathbf{S}_{IP} \\ \mathbf{S}_{OP} \end{pmatrix} + \mathbf{U}$$

$$\begin{pmatrix} \mathbf{S}_{IP} \\ \mathbf{S}_{OP} \end{pmatrix} = (\mathbf{R}^T\mathbf{R})^{-1}\mathbf{R}^T\mathbf{S}_{obs}$$

where $\mathbf{s}_{obs,j}$ (j = 1, 2, 3···) is a row vector that represents a transmission (single-beam) spectrum measured at a polarization angle of ϕ_j (j = 1, 2, 3, ...), the collection of $\mathbf{s}_{obs,j}$ vectors forms the matrix, and $\mathbf{S}_{obs}$. $\mathbf{S}_{IP}$ and $\mathbf{S}_{OP}$ are the decomposed IP and OP single-beam spectra, respectively. $r_{IP,j}$ (j = 1, 2, 3, ...) and $r_{OP,j}$ (j = 1, 2, 3, ...) are weighting coefficients for $\mathbf{S}_{IP}$ and $\mathbf{S}_{OP}$, respectively. For example, $\mathbf{s}_{obs,1}$ can be expressed as a linear combination of $\mathbf{S}_{IP}$ and $\mathbf{S}_{OP}$, as $\mathbf{s}_{obs,1} = r_{IP,1}\mathbf{S}_{IP} + r_{OP,1}\mathbf{S}_{OP}$. $\mathbf{R}$ is a matrix of weighting coefficients for $\mathbf{S}_{IP}$ and $\mathbf{S}_{OP}$. $\mathbf{U}$ is a matrix containing a nonlinear response to $\mathbf{R}$. Therefore, nonlinear noise factors (e.g., reflected IR light) are rejected in the classical least-squares regression calculation and pooled in $\mathbf{U}$ as the error.

For details of the deduction of $\mathbf{R}$, we refer interested readers to the original references.[32,34,36] In short, Shioya et al.[36] show that $\mathbf{R}$ depends on polarization angle ϕ, expressed as

$$\mathbf{R} = \begin{pmatrix} \gamma\cos^2\phi_1 + \sin^2\phi_1(\sin^2\theta\tan^2\theta + \cos^2\theta) & \sin^2\phi_1\tan^2\theta \\ \vdots & \vdots \end{pmatrix}$$

where γ is defined as the intensity ratio of the s-polarized light (S^s_{blank}) to the p-polarized light (S^p_{blank}) at a wavenumber when measured without a substrate (blank). In practice, γ can be calculated using the s- and p-polarized single-beam spectra of the background measurements with a substrate (S^s_{bg} and S^p_{bg}, respectively) and the transmittance of the substrate for the s- and p-polarized light (T^s_{sub} and T^p_{sub}, respectively) as

$$\gamma \equiv \frac{S^s_{blank}}{S^p_{blank}} = \frac{S^s_{bg}T^p_{sub}}{S^p_{bg}T^s_{sub}}$$

because $S^s_{bg} = S^s_{blank}T^s_{sub}$ and $S^p_{bg} = S^p_{blank}T^p_{sub}$. T^s_{sub} and T^p_{sub} can be calculated using the refractive index of the substrate (3.41 for Si).[30,34,62] After obtaining the IP and OP single-beam spectra ($\mathbf{S}_{IP}$ and $\mathbf{S}_{OP}$), the IP and OP absorbance spectra ($\mathbf{A}_{IP}$ and $\mathbf{A}_{OP}$) are calculated as

$$\mathbf{A}_{IP} = -\log\frac{\mathbf{S}^{sam}_{IP}}{\mathbf{S}^{bg}_{IP}}, \quad \mathbf{A}_{OP} = -\log\frac{\mathbf{S}^{sam}_{OP}}{\mathbf{S}^{bg}_{OP}}$$

where the superscripts bg and sam indicate background and sample measurements, respectively.

■ ASSOCIATED CONTENT

Supporting Information

The Supporting Information is available free of charge at https://pubs.acs.org/doi/10.1021/acs.jpclett.0c01585.

Typical single-beam spectra measured at an angle of incidence of 45° at various polarization angles from 0° (s-polarization) to 90° (p-polarization) in 15° steps before the MAIRS analysis (Figures S1 and S2); IP and OP spectra of the ν3 band of amorphous CH_4 at 6 K calculated assuming n = 1.33 (Figure S3); photograph of Si substrate connected with copper sample holder with indium solder by ultrasonic soldering (Figure S4); summary of A_{IP}, n^4HA_{OP}, $\sqrt{\frac{2A_{IP}}{n^4HA_{OP}}}$, and orientation angle α for the ν3 band of amorphous CH_4 on a Si substrate at 6 K (Table S1); summary of the dependence of the n (n^4H) value on A_{IP}, n^4HA_{OP}, $\sqrt{\frac{2A_{IP}}{n^4HA_{OP}}}$, and orientation angle α for the ν3 band of amorphous CH_4 on a Si substrate at 6 K (Table S2); summary of A_{IP}, n^4HA_{OP}, $\sqrt{\frac{2A_{IP}}{n^4HA_{OP}}}$, and orientation angle α for the $^{14}N^{14}NO$ ν3 band of amorphous N_2O on a Si substrate at 6 K (Table S3) (PDF)

■ AUTHOR INFORMATION

Corresponding Author

Tetsuya Hama − *Komaba Institute for Science and Department of Basic Science, The University of Tokyo, Meguro, Tokyo 153-8902, Japan;* orcid.org/0000-0002-4991-4044; Phone: +81-3-5465-8917; Email: hamatetsuya@g.ecc.u-tokyo.ac.jp

https://dx.doi.org/10.1021/acs.jpclett.0c01585
J. Phys. Chem. Lett. 2020, 11, 7857−7866

Authors

Atsuki Ishibashi − *Institute of Low Temperature Science, Hokkaido University, Sapporo 060-0819, Japan*

Akira Kouchi − *Institute of Low Temperature Science, Hokkaido University, Sapporo 060-0819, Japan*

Naoki Watanabe − *Institute of Low Temperature Science, Hokkaido University, Sapporo 060-0819, Japan;* orcid.org/0000-0001-8408-2872

Nobutaka Shioya − *Institute for Chemical Research, Kyoto University, Uji, Kyoto 611-0011, Japan*

Takafumi Shimoaka − *Institute for Chemical Research, Kyoto University, Uji, Kyoto 611-0011, Japan;* orcid.org/0000-0001-9131-9831

Takeshi Hasegawa − *Institute for Chemical Research, Kyoto University, Uji, Kyoto 611-0011, Japan;* orcid.org/0000-0001-5574-9869

Complete contact information is available at: https://pubs.acs.org/10.1021/acs.jpclett.0c01585

Notes

The authors declare no competing financial interest.

■ ACKNOWLEDGMENTS

We thank our colleagues Dr. Hiroshi Hidaka, Dr. Yuki Kimura, Dr. Yasuhiro Oba, and Dr. Tomoya Yamazaki at the Institute of Low Temperature Science, Hokkaido University. This work was supported by JSPS Kakenhi Grant Numbers 18H01262 and 19K22901.

■ REFERENCES

(1) Kubono, A.; Okui, N. Polymer Thin Films Prepared by Vapor Deposition. *Prog. Polym. Sci.* **1994**, *19* (3), 389−438.

(2) Rossnagel, S. M. Thin Film Deposition with Physical Vapor Deposition and Related Technologies. *J. Vac. Sci. Technol., A* **2003**, *21* (5), S74−S87.

(3) Shioya, N.; Murdey, R.; Nakao, K.; Yoshida, H.; Koganezawa, T.; Eda, K.; Shimoaka, T.; Hasegawa, T. Alternative Face-on Thin Film Structure of Pentacene. *Sci. Rep.* **2019**, *9* (1), 579.

(4) Hama, T.; Watanabe, N. Surface Processes on Interstellar Amorphous Solid Water: Adsorption, Diffusion, Tunneling Reactions, and Nuclear-Spin Conversion. *Chem. Rev.* **2013**, *113* (12), 8783−8839.

(5) Tielens, A. G. G. M. The Molecular Universe. *Rev. Mod. Phys.* **2013**, *85* (3), 1021−1081.

(6) Boogert, A. C. A.; Gerakines, P. A.; Whittet, D. C. B. Observations of the Icy Universe. *Annu. Rev. Astron. Astrophys.* **2015**, *53*, 541−581.

(7) Elliott, E.; Pritchard, T.; Hampshire, M.; Tomlinson, R. Charge Build-up in Ice Layers Condensing on Liquid Nitrogen Traps. *Vacuum* **1969**, *19* (8), 366.

(8) Kutzner, K. Spontaneous Polarization of Condensing Carbon Monoxide and Other Gases with an Electrical Dipole Moment. *Thin Solid Films* **1972**, *14* (1), 49−61.

(9) Onsager, L.; Staebler, D. L.; Mascarenhas, S. Electrical Effects during Condensation and Phase Transitions of Ice. *J. Chem. Phys.* **1978**, *68* (8), 3823−3828.

(10) Chrzanowski, J.; Sujak, B. The Electret Effect in Polar Molecule Condensates in the Temperature Range 90−230 K. *Thin Solid Films* **1981**, *79* (2), 101−111.

(11) Bu, C.; Shi, J.; Raut, U.; Mitchell, E. H.; Baragiola, R. A. Effect of Microstructure on Spontaneous Polarization in Amorphous Solid Water Films. *J. Chem. Phys.* **2015**, *142* (13), 134702.

(12) Lasne, J.; Rosu-Finsen, A.; Cassidy, A.; McCoustra, M. R. S.; Field, D. Spontaneous Electric Fields in Solid Carbon Monoxide. *Phys. Chem. Chem. Phys.* **2015**, *17* (44), 30177−30187.

(13) Balog, R.; Cicman, P.; Jones, N. C.; Field, D. Spontaneous Dipole Alignment in Films of N_2O. *Phys. Rev. Lett.* **2009**, *102* (7), 073003.

(14) Plekan, O.; Cassidy, A.; Balog, R.; Jones, N. C.; Field, D. A New Form of Spontaneously Polarized Material. *Phys. Chem. Chem. Phys.* **2011**, *13* (47), 21035−21044.

(15) Cassidy, A.; Plekan, O.; Balog, R.; Jones, N. C.; Field, D. Spontaneous Electric Fields in Films of CF_3Cl, CF_2Cl_2 and $CFCl_3$. *Phys. Chem. Chem. Phys.* **2013**, *15* (1), 108−113.

(16) Plekan, O.; Cassidy, A.; Balog, R.; Jones, N. C.; Field, D. Spontaneous Electric Fields in Films of Cis-Methyl Formate. *Phys. Chem. Chem. Phys.* **2012**, *14* (28), 9972−9976.

(17) Roman, M.; Dunn, A.; Taj, S.; Keolopile, Z. G.; Rosu-Finsen, A.; Gutowski, M.; McCoustra, M. R. S.; Cassidy, A. M.; Field, D. Assigning a Structural Motif Using Spontaneous Molecular Dipole Orientation in Thin Films. *Phys. Chem. Chem. Phys.* **2018**, *20* (46), 29038−29044.

(18) Field, D.; Plekan, O.; Cassidy, A.; Balog, R.; Jones, N. C.; Dunger, J. Spontaneous Electric Fields in Solid Films: Spontelectrics. *Int. Rev. Phys. Chem.* **2013**, *32* (3), 345−392.

(19) Sobolewski, W. J. Electrical Effects Accompanying the Phase Transitions in Ethanol Cryocondensed Thin Layers. *Phase Transitions* **1997**, *62* (1−2), 95−104.

(20) Gavra, I. K.; Pilidi, A. N.; Tsekouras, A. A. Spontaneous Polarization of Vapor-Deposited 1-Butanol Films and Its Dependence on Temperature. *J. Chem. Phys.* **2017**, *146* (10), 104701.

(21) Pilidi, A. N.; Gavra, I. K.; Tsekouras, A. A. Spontaneous Polarization of Cryo-Deposited Films for Five Normal Saturated Monohydroxy Alcohols, $C_nH_{2n+1}OH$, n = 1−5. *J. Phys. Chem. B* **2019**, *123* (40), 8505−8511.

(22) Plekan, O.; Rosu-Finsen, A.; Cassidy, A. M.; Lasne, J.; McCoustra, M. R. S.; Field, D. A Review of Recent Progress in Understanding the Spontelectric State of Matter. *Eur. Phys. J. D* **2017**, *71* (6), 162.

(23) Cassidy, A.; Plekan, O.; Dunger, J.; Balog, R.; Jones, N. C.; Lasne, J.; Rosu-Finsen, A.; McCoustra, M. R. S.; Field, D. Investigations into the Nature of Spontelectrics: Nitrous Oxide Diluted in Xenon. *Phys. Chem. Chem. Phys.* **2014**, *16* (43), 23843−23853.

(24) Cassidy, A.; Plekan, O.; Balog, R.; Dunger, J.; Field, D.; Jones, N. C. Electric Field Structures in Thin Films: Formation and Properties. *J. Phys. Chem. A* **2014**, *118* (33), 6615−6621.

(25) Lasne, J.; Rosu-Finsen, A.; Cassidy, A.; McCoustra, M. R. S.; Field, D. Spontaneously Electrical Solids in a New Light. *Phys. Chem. Chem. Phys.* **2015**, *17* (32), 20971−20980.

(26) Cassidy, A.; Jørgensen, M. R. V.; Rosu-Finsen, A.; Lasne, J.; Jørgensen, J. H.; Glavic, A.; Lauter, V.; Iversen, B. B.; McCoustra, M. R. S.; Field, D. Dipole-Oriented Molecular Solids Can Undergo a Phase Change and Still Maintain Electrical Polarization. *J. Phys. Chem. C* **2016**, *120* (42), 24130−24136.

(27) Cassidy, A.; James, R. L.; Dawes, A.; Lasne, J.; Field, D. The Optical Absorption Spectra of Spontaneously Electrical Solids: The Case of Nitrous Oxide. *Phys. Chem. Chem. Phys.* **2019**, *21* (3), 1190−1197.

(28) Rosu-Finsen, A.; Lasne, J.; Cassidy, A.; McCoustra, M. R. S.; Field, D. Spontaneous Polarization of Solid CO on Water Ices and Some Astrophysical Implications. *Phys. Chem. Chem. Phys.* **2016**, *18* (7), 5159−5171.

(29) Tolstoy, V. P.; Chernyshova, I. V.; Skryshevsky, V. A. *Handbook of Infrared Spectroscopy of Ultrathin Films*; John Wiley & Sons: Hoboken, NJ, 2003.

(30) Hasegawa, T. *Quantitative Infrared Spectroscopy for Understanding of a Condensed Matter*; Springer Japan: Tokyo, 2017.

(31) Hasegawa, T.; Shioya, N. MAIRS: Innovation of Molecular Orientation Analysis in a Thin Film. *Bull. Chem. Soc. Jpn.* **2020**, DOI: 10.1246/bcsj.20200139.

(32) Hasegawa, T. A Novel Measurement Technique of Pure Out-of-Plane Vibrational Modes in Thin Films on a Nonmetallic Material with No Polarizer. *J. Phys. Chem. B* **2002**, *106* (16), 4112−4115.

(33) Hasegawa, T. A. New Spectroscopic Tool for Surface Layer Analysis: Multiple-Angle Incidence Resolution Spectrometry. *Anal. Bioanal. Chem.* **2007**, *388* (1), 7−15.
(34) Itoh, Y.; Kasuya, A.; Hasegawa, T. Analytical Understanding of Multiple-Angle Incidence Resolution Spectrometry Based on a Classical Electromagnetic Theory. *J. Phys. Chem. A* **2009**, *113* (27), 7810−7817.
(35) Shioya, N.; Shimoaka, T.; Murdey, R.; Hasegawa, T. Accurate Molecular Orientation Analysis Using Infrared P-Polarized Multiple-Angle Incidence Resolution Spectrometry (pMAIRS) Considering the Refractive Index of the Thin Film Sample. *Appl. Spectrosc.* **2017**, *71* (6), 1242−1248.
(36) Shioya, N.; Tomita, K.; Shimoaka, T.; Hasegawa, T. Second Generation of Multiple-Angle Incidence Resolution Spectrometry. *J. Phys. Chem. A* **2019**, *123* (32), 7177−7183.
(37) Satorre, M. Á.; Domingo, M.; Millán, C.; Luna, R.; Vilaplana, R.; Santonja, C. Density of CH_4, N_2 and CO_2 Ices at Different Temperatures of Deposition. *Planet. Space Sci.* **2008**, *56* (13), 1748−1752.
(38) Gerakines, P. A.; Hudson, R. L. Infrared Spectra and Optical Constants of Elusive Amorphous Methane. *Astrophys. J., Lett.* **2015**, *805* (2), No. L20.
(39) Hudson, R. L.; Loeffler, M. J.; Gerakines, P. A. Infrared Spectra and Band Strengths of Amorphous and Crystalline N_2O. *J. Chem. Phys.* **2017**, *146* (2), 024304.
(40) Brunetto, R.; Caniglia, G.; Baratta, G. A.; Palumbo, M. E. Integrated Near-Infrared Band Strengths of Solid CH_4 and Its Mixtures with N_2. *Astrophys. J.* **2008**, *686* (2), 1480−1485.
(41) Molpeceres, G.; Satorre, M. A.; Ortigoso, J.; Zanchet, A.; Luna, R.; Millán, C.; Escribano, R.; Tanarro, I.; Herrero, V. J.; Maté, B. Physical and Spectroscopic Properties of Pure C_2H_4 and CH_4:C_2H_4 Ices. *Mon. Not. R. Astron. Soc.* **2017**, *466* (2), 1894−1902.
(42) Molpeceres, G.; Satorre, M. A.; Ortigoso, J.; Millán, C.; Escribano, R.; Maté, B. Optical Constants and Band Strengths of CH_4:C_2H_6 Ices in the Near- and Mid-Infrared. *Astrophys. J.* **2016**, *825* (2), No. 156.
(43) Shioya, N.; Norimoto, S.; Izumi, N.; Hada, M.; Shimoaka, T.; Hasegawa, T. Optimal Experimental Condition of IR pMAIRS Calibrated by Using an Optically Isotropic Thin Film Exhibiting the Berreman Effect. *Appl. Spectrosc.* **2017**, *71* (5), 901−910.
(44) Popenoe, D. D.; Stole, S. M.; Porter, M. D. Optical Considerations for Infrared Reflection Spectroscopic Analysis in the C-H Stretching Region of Monolayer Films at an Aqueous/Metal Interface. *Appl. Spectrosc.* **1992**, *46* (1), 79−87.
(45) Hasegawa, T. A. New Approach to Analysis of Molecular Structure in Thin Films: Infrared Multiple-Angle Incidence Resolution Spectrometry. *Appl. Spectrosc. Rev.* **2008**, *43* (3), 181−201.
(46) Ovchinnikov, M. A.; Wight, C. A. Dipole Mechanism of Line Broadening in Amorphous Solids. *J. Chem. Phys.* **1995**, *102* (1), 67−74.
(47) Nagai, N.; Okada, H.; Hasegawa, T. Morphology-Sensitive Infrared Absorption Bands of Polymers Derived from Surface Polaritons. *AIP Adv.* **2019**, *9* (10), 105203.
(48) Fukumi, A.; Shimoaka, T.; Shioya, N.; Nagai, N.; Hasegawa, T. Infrared Active Surface Modes Found in Thin Films of Perfluoroalkanes Reveal the Dipole − Dipole Interaction and Surface Morphology. *J. Chem. Phys.* **2020**, *153*, 044703.
(49) Junk, G.; Svec, H. J. The Absolute Abundance of the Nitrogen Isotopes in the Atmosphere and Compressed Gas from Various Sources. *Geochim. Cosmochim. Acta* **1958**, *14* (3), 234−243.
(50) Peterson, O. G.; Batchelder, D. N.; Simmons, R. O. Measurements of X-Ray Lattice Constant, Thermal Expansivity, and Isothermal Compressibility of Argon Crystals. *Phys. Rev.* **1966**, *150* (2), 703−711.
(51) Matsuzaki, F.; Inaoka, K.; Okada, M.; Sato, K. Molecular Orientation in Physical-Vapour Deposition of Long-Chain Stearic Acid. *J. Cryst. Growth* **1984**, *69* (2−3), 231−240.
(52) Tanaka, K.; Okui, N.; Sakai, T. Molecular Orientation Behavior of Paraffin Thin Films Made by Vapor Deposition. *Thin Solid Films* **1991**, *196* (1), 137−145.
(53) Hama, T.; Ishizuka, S.; Yamazaki, T.; Kimura, Y.; Kouchi, A.; Watanabe, N.; Sugimoto, T.; Pirronello, V. Fast Crystalline Ice Formation at Extremely Low Temperature through Water/Neon Matrix Sublimation. *Phys. Chem. Chem. Phys.* **2017**, *19* (27), 17677−17684.
(54) Crusius, J. P.; Hellmann, R.; Hassel, E.; Bich, E. Ab Initio Intermolecular Potential Energy Surface and Thermophysical Properties of Nitrous Oxide. *J. Chem. Phys.* **2015**, *142* (24), 244307.
(55) Noble, J. A.; Congiu, E.; Dulieu, F.; Fraser, H. J. Thermal Desorption Characteristics of CO, O_2 and CO_2 on Non-Porous Water, Crystalline Water and Silicate Surfaces at Submonolayer and Multilayer Coverages. *Mon. Not. R. Astron. Soc.* **2012**, *421* (1), 768−779.
(56) Luna, R.; Domingo, M.; Millán, C.; Santonja, C.; Satorre, M. Study of the Frequency Factor in the Thermal Desorption of Astrophysical Ice Analogs: CH_4, C_2H_4, C_2H_6, CH_3OH, CO, CO_2, H_2O and N_2. *Vacuum* **2018**, *152*, 278−284.
(57) Ekin, J. W. *ExperimentalTechniques for Low-Temperature Measurements: Cryostat Design, Material Properties, and Superconductor Critical-Current Testing*; Oxford University Press: New York, 2006.
(58) Nakao, F. Determination of the Ionization Gauge Sensitivity Using the Relative Ionization Cross-Section. *Vacuum* **1975**, *25* (9−10), 431−435.
(59) Schallamach, A. X-Ray Investigation of the Structure Transition of Methane at the λ Point. *Proc. R. Soc. London. Ser. A. Math. Phys. Sci.* **1939**, *171* (947), 569−578.
(60) Hamilton, W. C.; Petrie, M. Confirmation of Disorder in Solid Nitrous Oxide by Neutron Diffraction. *J. Phys. Chem.* **1961**, *65* (8), 1453−1454.
(61) Hasegawa, T. Advanced Multiple-Angle Incidence Resolution Spectrometry for Thin-Layer Analysis on a Low-Refractive-Index Substrate. *Anal. Chem.* **2007**, *79* (12), 4385−4389.
(62) *Introduction to Experimental Infrared Spectroscopy: Fundamentals and Practical Methods*; Tasumi, M., Ed.; John Wiley & Sons: Chichester, 2014.

https://dx.doi.org/10.1021/acs.jpclett.0c01585
J. Phys. Chem. Lett. 2020, 11, 7857−7866